Chapter 4

Practical Implementation of Semiactive Skyhook Control

This chapter will address some of the issues concerning the practical implementation of a semiactive skyhook system. In particular, it addresses the application of a semiactive skyhook controller to a seat suspension system for heavy trucks. It evaluates the dynamic responses of the semiactive system, analyzes dynamic phenomena inherent with the semiactive skyhook system, and offers modifications to the skyhook policy to further improve the dynamic responses of the suspension system.

4.1 Dynamic System Description

The dynamic system that was evaluated in this chapter included the seat suspension, shown in Fig. 4.1, commonly used in heavy truck vehicles for improving operator comfort. The seat is an Isringhausen model 8000 with a scissors-type suspension, as shown in Fig. 4.2.

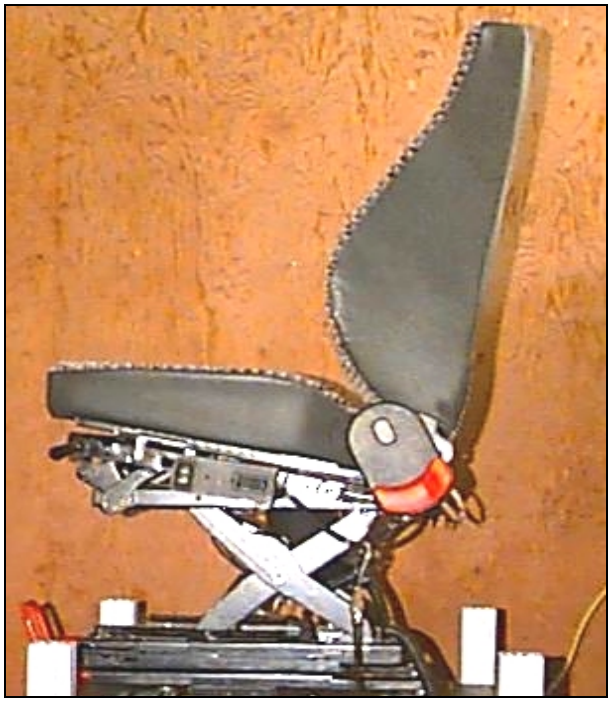

Figure 4.1 Isringhausen Seat Suspension
at the Advanced Vehicle Dynamics Laboratory (AVDL) of Virginia Tech

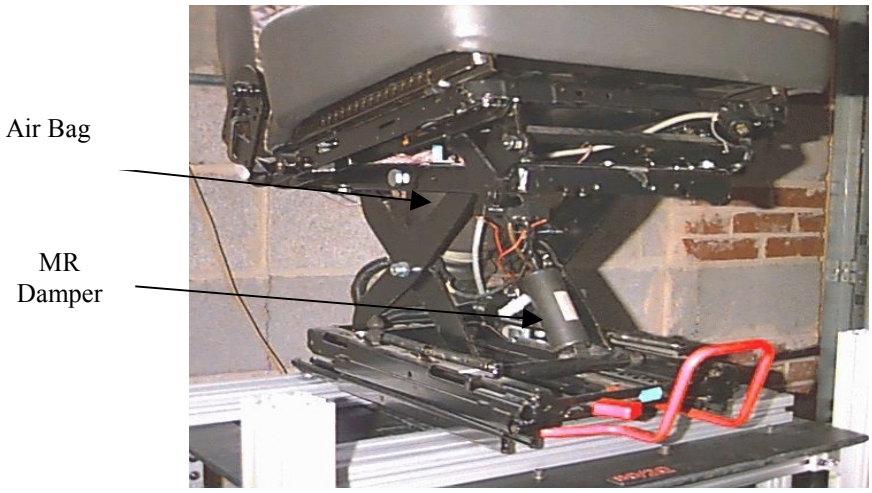

(a)

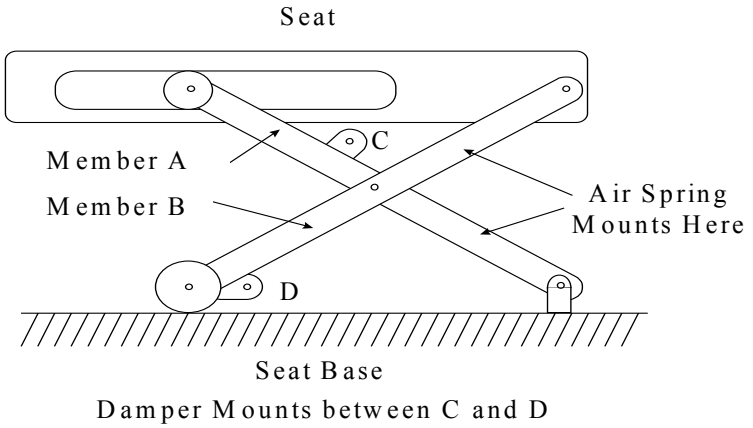

(b)

Figure 4.2 Isringhausen Seat Suspension:
(a) Close-up of Seat Suspension; (b) Schematic of Scissors Seat Suspension

The dynamic control system uses dSPACE for the hardware-in-the-loop testing. dSPACE is composed of both commercial software and hardware, and uses Simulink to implement closed-loop control on an experimental system. The Simulink block diagram is compiled and downloaded into a DSP chip for real-time control purposes.

The hardware portion of the dSPACE consists of an AutoBox, shown in Fig. 4.3. The AutoBox contains the DSP processor board, where the control program resides, an I/O card with up to 20 inputs and 8 outputs for sensor and actuator connections, and a power supply. Since the AutoBox is designed for portable vehicle control development, the

power supply consists of a DC/DC converter that allows the AutoBox to be powered directly from a vehicle 12-volt system.

Figure 4.3 dSPACE AutoBox

4.2 Skyhook Controller Implementation

As described in Chapter 2, skyhook control is based on two velocity signals, relative velocity and absolute velocity. In the seat suspension, an accelerometer and an LVDT are used to measure the seat acceleration and the relative displacement, respectively. These signals must be changed to the velocities necessary for skyhook controls through proper algorithms.

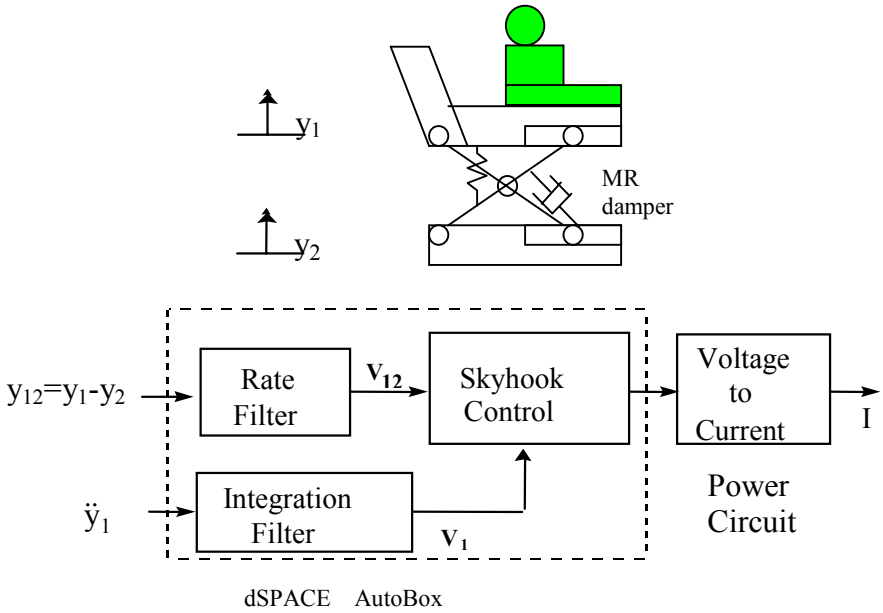

Figure 4.4 Implementation of Skyhook Control on Seat Suspension

As shown in Fig. 4.4, y_{12} and $\ddot{y}_1$ represent the seat relative displacement and the absolute acceleration, respectively. A rate filter is used to differentiate y_{12} to get the estimate of the relative velocity v_{12}, while an integration filter obtains the seat absolute velocity v_1 from the seat acceleration $\ddot{y}_1$. Both filters are implemented in the AutoBox, and the filtered velocity signals are used in the skyhook control to determine the control voltage. Through a power stage circuit, the control voltage is transferred to the corresponding current I for the MR damper.

Since an MR damper is used in the seat suspension, the damping level can be changed according to the current I supplied to the damper. The current I, which is determined according to skyhook control, can be decided by

$$I = \begin{cases} K|v_1| & v_{12}v_1 \geq 0 \\ 0 & v_{12}v_1 < 0 \end{cases} \tag{4.1}$$

where K is a constant gain. The details of both filters and the laboratory setup will be discussed in the following sections.

4.2.1 Integration Filter Design

One signal used in the skyhook control is the seat velocity v_1 (i.e., the velocity of the suspended body). The velocity signal can be obtained through the integration of the corresponding acceleration. In the Simulink program, an integration filter is designed to achieve proper integration. In addition, the integral filter $T_I(s)$ must be able to eliminate the DC component in the measured acceleration. Thus, the filter has a transfer function defined by

$$T_I(s) = \frac{0.056s}{0.056s^2 + 1.0560s + 1} \tag{4.2}$$

The Bode plot shown in Fig. 4.5 indicates that at frequencies above 10 Hz the filter causes about 90 degree phase shift to the input signal. Therefore, it works as an

integrator, although it can cause a phase error in comparison with an ideal integrator that require a 90 drgree phase shift at any frequency. The phase error induced from the estimate, however, does not deterioate the skyhook performance, as will be discussed in more detail in Section 4.3.2.1.

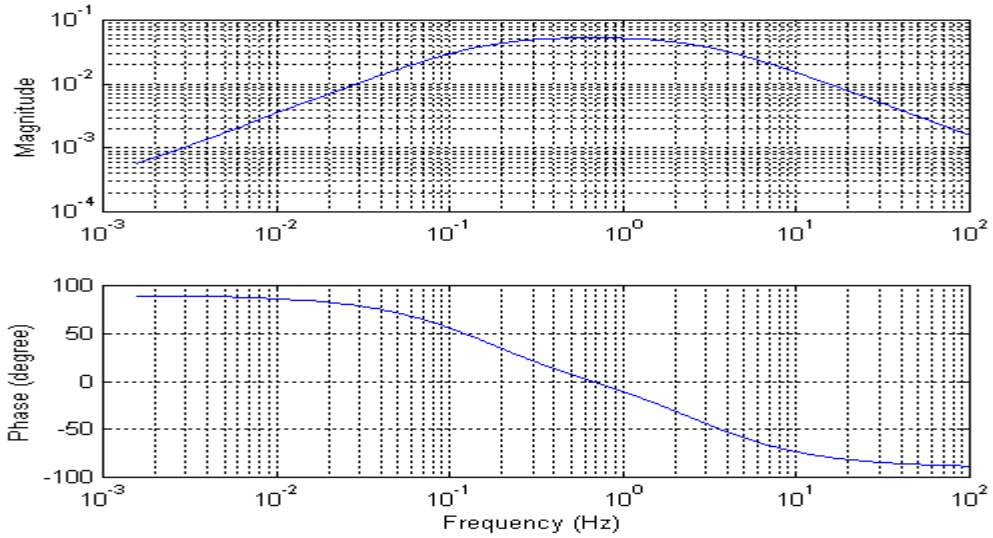

Figure 4.5 Bode Plot of the Integration Filter

4.2.2 Rate Filter Design

In order to get the estimate of the relative velocity v_{12}, a high pass filter is designed to defferentiate the relative displacement y_{12}, as shown in Eq. (4.3),

$$v_{12}(k) = G[H(y_{12}(k) - y_{12}(k-1)) + v_{12}(k-1)] \tag{4.3}$$

to derive the relative velocity for the skyhook control policy. In Eq. (4.3), G and H are constants, y_{12} is the measured relative displacement and v_{12} is the estimate of the relative velocity.

Next, we will analyze the rate filter of Eq. (4.3). This filter was selected by Lord Corporation engineers for implementation on their semiactive seat suspension system. In the z-domain we have

$$v_{12}(k)(1-Gz^{-1}) = GH(1-z^{-1})y_{12}(k)$$

where z is the Z-domain operator, G and H are constants, y_{12} is the relative displacement and v_{12} is the estimate of the relative velocity.

We analyze the performnace of the filter by transforming its formulation from Z-domain to S-domain by rewriting the above equation as

$$\frac{v_{12}(k)}{y_{12}(k)} = \frac{GH(1-z^{-1})}{(1-Gz^{-1})} = \frac{GH[(z-1)/T]}{(z-1)/T + (1-G)/T} \tag{4.4}$$

where T the sampling period.

Furthermore, assuming that the sampling frequency (1/T) is high enough compared with the frequency range of the dynamic systems, we can use the forward rule

$$s = \frac{z-1}{T} \tag{4.5}$$

Combining Eqs. (4.4) and (4.5) yields the rate filter in the S-domain

$$\frac{v_{12}(s)}{y_{12}(s)} = \frac{GHs}{s + (1-G)/T} \tag{4.6}$$

Typically a high pass filter is used as differntiator for the low frequency range. A nomial high pass filter is

$$H(s) = (1/\tau)\frac{s}{s+1/\tau} \tag{4.7}$$

where the time constant τ is defined as

$$\tau = 1/(2\pi f)$$

and f is the break frequency of Eq. (4.7) [8, 20]. Comparing Eqs. (4.6) and (4.7) yields

$$G = 1 - 2\pi fT$$
$$H = 2\pi f / G \tag{4.8}$$

Equation (4.8) indicates that if G, H, and the sampling period T are known, then we can calculate the break frequency f of the rate filter. For G = 0, the digital filter becomes degenerated. As shown on the Bode plots in Fig. 4.6, the filter break frequency has a different effect on the output signal.

In order to check the effect of the break frequency on the estimate, a cosine displacement signal with 1.8 Hz is used to test the rate filter of Eq. (4.3). The true velocity is a corresponding sine signal. The true velocity and the estimates resulting from rate filters with break frequency of 4 and 10 Hz are shown in Fig. 4.7. The figure indicates that the

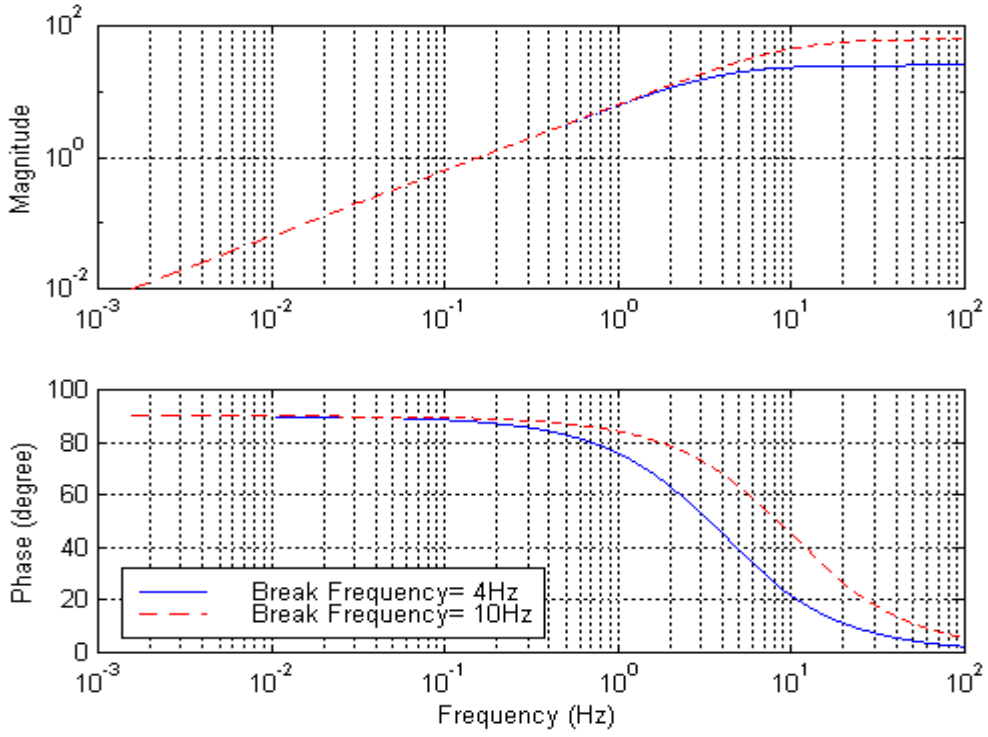

Figure 4.6 Effect of Break Frequency on Phase and Gain of Rate Filter

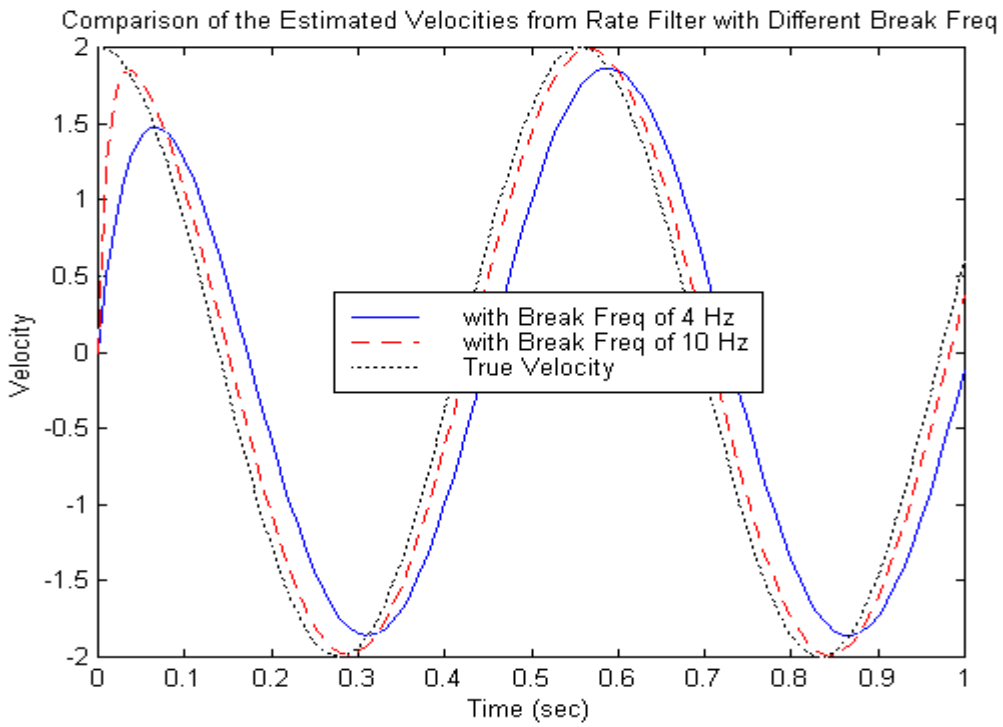

Figure 4.7 Comparison of Estimated Velocities with the True Velocity for a 1.8 Hz Pure Tone Displacement Signal

rate filter with a higher break frequency can give a more accurate estimate of the velocity. The filter with a lower break frequency causes the estimate to be less accurate in both amplitude and phase. The phase errors can cause performance deterioration in skyhook control. For our systems, we selected the filter break frequency to be substantially higher than the dynamic range of the system, in order to minimize the distortion effects of the filter.

4.2.3 Simulink Control Program

The Simulink block diagrams are shown in Figs. 4.8-4.11. The block diagrams include the interface to the measurement sensors and the control output. They also include several other function blocks, including a rate filter, and the "hook controller" block that is composed of integration filters and a skyhook/groundhook [27] block. In the control block diagram (Fig. 4.8), four different variations of skyhook control are included for use in studies beyond this dissertation. They include skyhook, groundhook, no-jerk skyhook, and no-jerk groundhook, as will be discussed in more depth in Section 4.4.

In the real time control system, two signals of the seat acceleration and relative displacement are measured. As shown in Fig. 4.8, the measurement sinals from the acclerometer and LVDT go through the "measurement" block to obtain the corresponding acceleration and relative displacement signals for the "hook controller" block. As described before, both signals have to be processed to the corresponding velocity signals for the skyhook control. Furthermore, since the damping level of an MR damper is dependent on the input current, the implementation of skyhook control for magneto-reological dampers can be

$$I = \begin{cases} K \mid v_1 \mid & v_1 v_{12} \geq 0 \\ 0 & v_1 v_{12} < 0 \end{cases} \tag{4.9}$$

where I is the current to the MR damper and K is a constant gain. The control current I is supplied to the MR damper through the power stage circuit which interfaces to the dSPACE AutoBox.

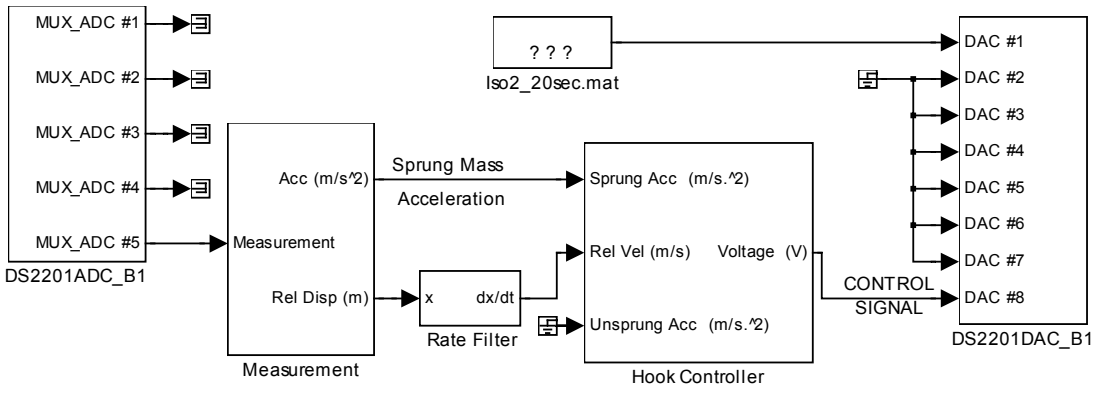

Figure 4.8 Simulink Block Diagram for the Semiactive Control

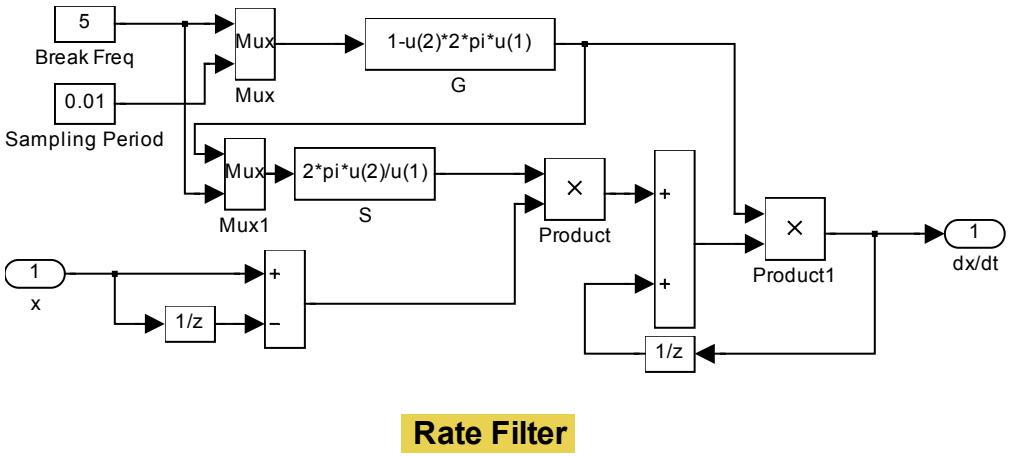

Figure 4.9 Simulink Block Diagram of the Rate Filter

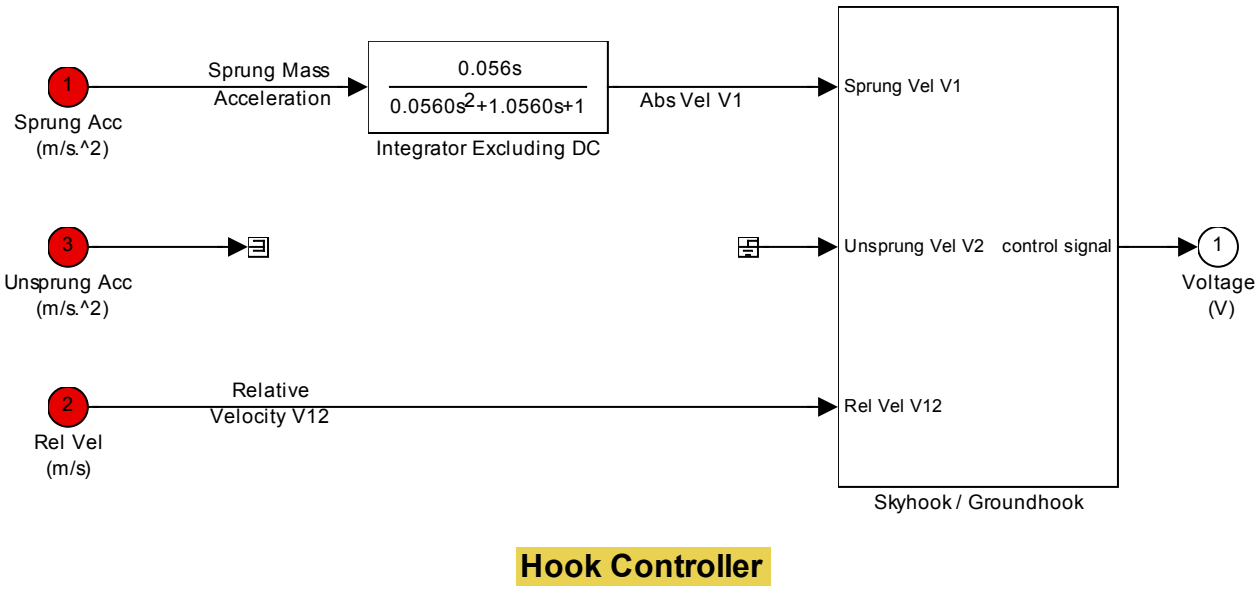

Figure 4.10 Simulink Block Diagram Program of Hook Controller

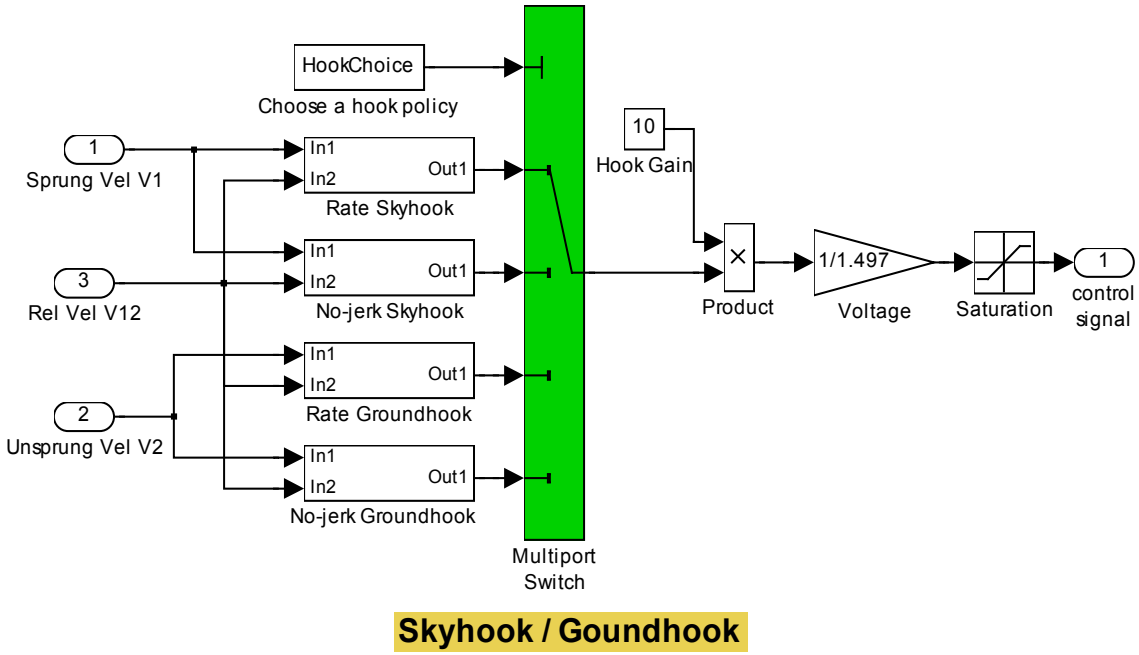

Figure 4.11 Simulink Block Diagram of Skyhook and Groundhook

4.2.4 ISO2 Base Excitation

For testing purposes, different excitation signals were considered, such as pure tone signal, and ISO2. ISO [71,72] is specified by the International Standard Organization, and it is usually used as test input for products that relate to human comfort, such as seat suspensions. As shown in Figs. 4.12 and 4.13, ISO2 is a broadband random excitation signal with an acceleration power spectrum that spreads from approximately 1 to 3 Hz.

The excitation signal can be created with Simulink, and the data file can be downloaded to the dSPACE AutoBox. According to the hardware-in-the-loop systems shown in Appendix A, the excitation signal is supplied to the MTS Controller. The hydraulic actuator vibrates the seat suspension according to the designed excitation.

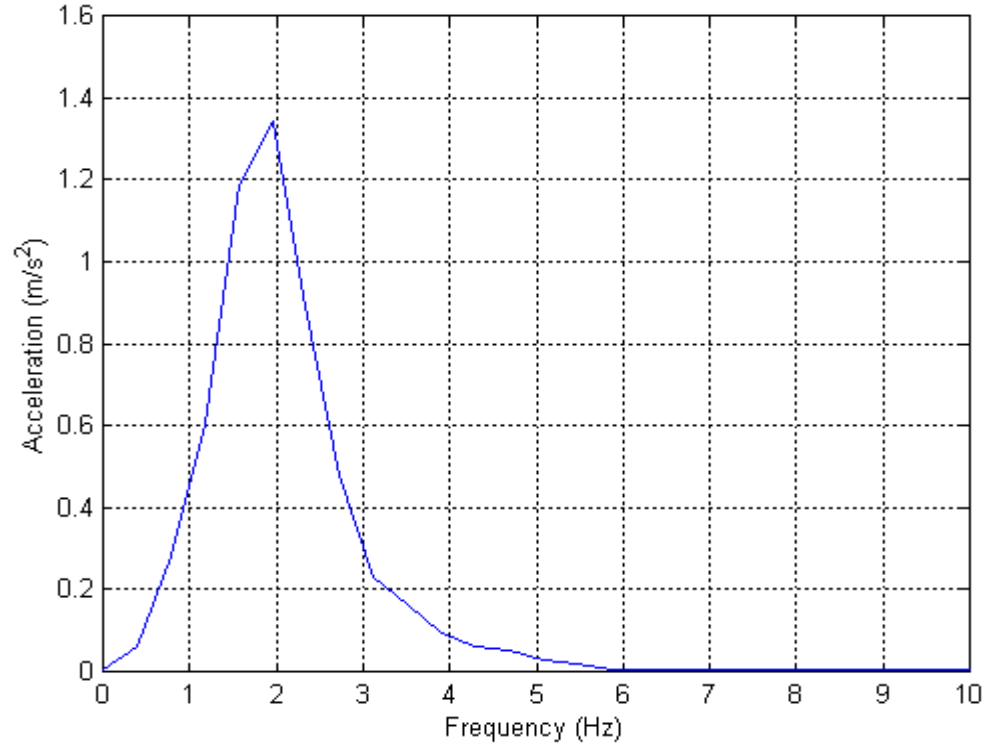

Figure 4.12 Power Spectrum of ISO2 Excitation

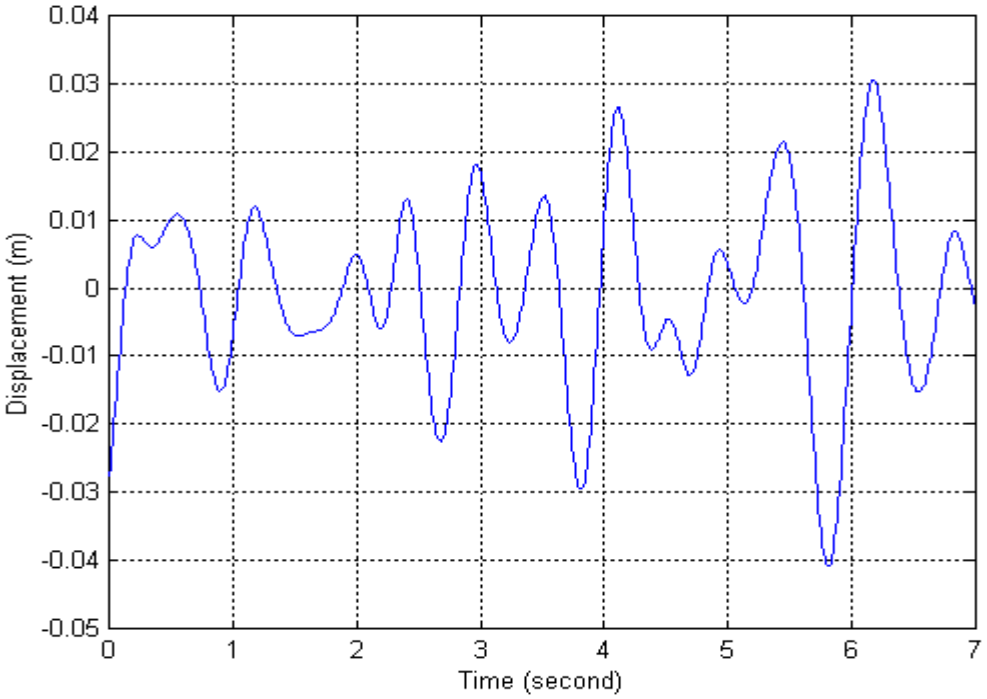

Figure 4.13 A Sample Time History of ISO2 Displacement

4.2.5 Laboratory Setup

The setup of the seat suspension for testing consists of four parts, as shown in Fig. A.1. Although the details of the experimental setup are included in Appendix A, we will next provide a brief description of the setup.

The Isringhausen seat suspension includes an air spring and an MR damper, as shown in Fig. 4.1. The dSPACE AutoBox is used as a real-time controller. It receives the sensory information and gives out a control signal. The dSPACE software of TRACE and COCKPIT in PC can communicate with the AutoBox. COCKPIT is used to adjust the values of real-time controller parameters. TRACE has two main fuctions; it provides graphic presentation of the sampled data on-line, and acquires the data. Finally, the hydraulic actuation system consists of a 2000 lb hydraulic actuator and a hydraulic controller that is used to operate and monitor the hydraulic system. The actuator input is provided by the AutoBox through the hydraulic controller.

4.3 System Dynamic Responses

For our dynamic testing, the vehicle seat suspension employed skyhook control, as described in Eq. (4.9). The data was collected through the dSPACE TRACE. The experimental data was used to analyze the nonlinearities of the semiactive skyhook control in both frequency and time domain. Furthermore, we set the break frequency of the rate filter to 4 Hz and the control system sampling frequency to 100 Hz.

4.3.1 Analysis of Experimental Data in Frequency Domain

We will first present an analysis of the seat acceleration data for ISO2 excitation in the frequency domain. Next, in order to clarify our observations, we present the seat responses to a pure tone excitation.

4.3.1.1 Observations in Frequency Domain

The seat acceleration power spectrum due to an ISO2 excitation is shown in Fig. 4.14. Figure 4.14 shows that there are two peaks in the seat acceleration. One is near the resonant frequency, 1.4 Hz, and the other approximately at 4.2 Hz, three times the

resonant frequency. ISO2, as shown in Fig. 4.12, has only one peak, approximately at 2 Hz. Therefore, the question to be answered is what causes the 4.2 Hz frequency, which we will refer to as the "higher harmonics".

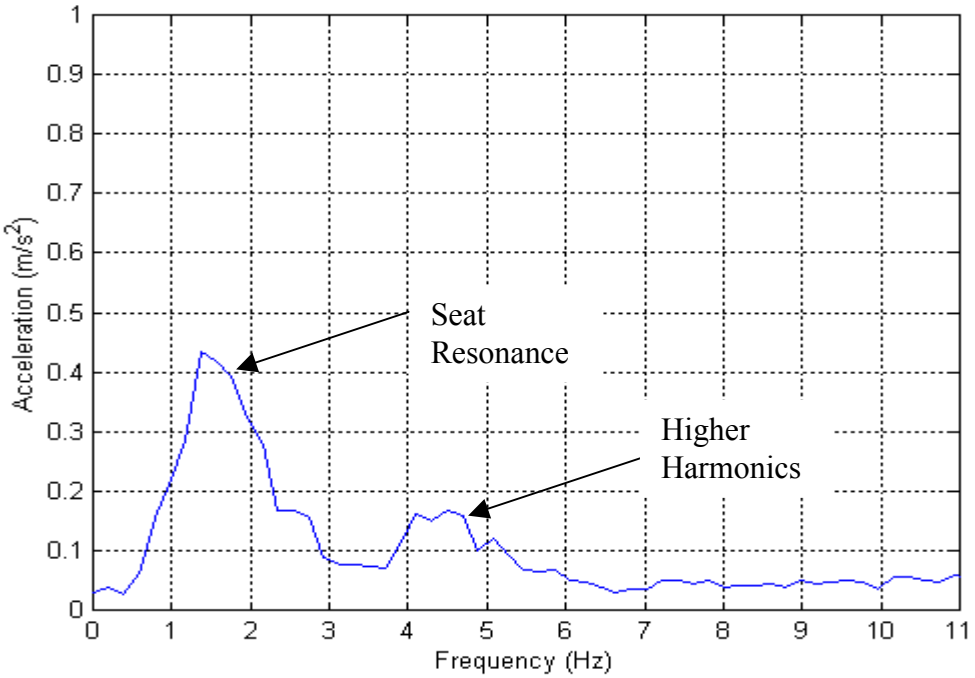

Figure 4.14 The Seat Acceleration with ISO2 Excitation in Frequency Domain

4.3.1.2 Analysis of Higher Harmonics

In order to make it easy to understand the dynamic responses, we apply a pure tone signal of 1.4 Hz to excite the seat suspension. Three different cases are tested: skyhook, soft damping, and hard damping. The soft and hard damping are created by providing 0.1 A and 1 A of currents to the damper, respectively. The frequency spectrum of the seat accelerations for the three cases are shown in Fig. 4.15. In addition, the currents to the damper in time and frequency domain are presented in Figs. 4.16 and 4.17, respectively.

Figure 4.15 clearly shows the presence of the higher harmonics at 4.2 Hz, 7 Hz, and 9.8 Hz – all odd multiples of the resonance frequency 1.4 Hz. No higher harmonics are observed for the soft and hard damping.

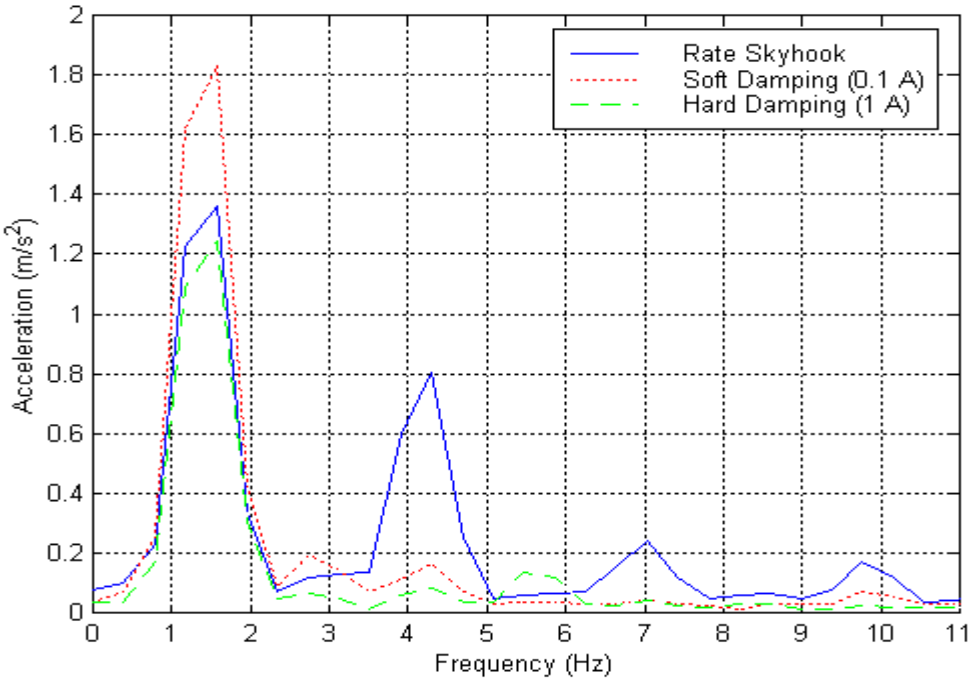

Figure 4.15 Acceleration Frequency Spectrum
for Skyhook and Passive Damping with Pure Tone Excitation

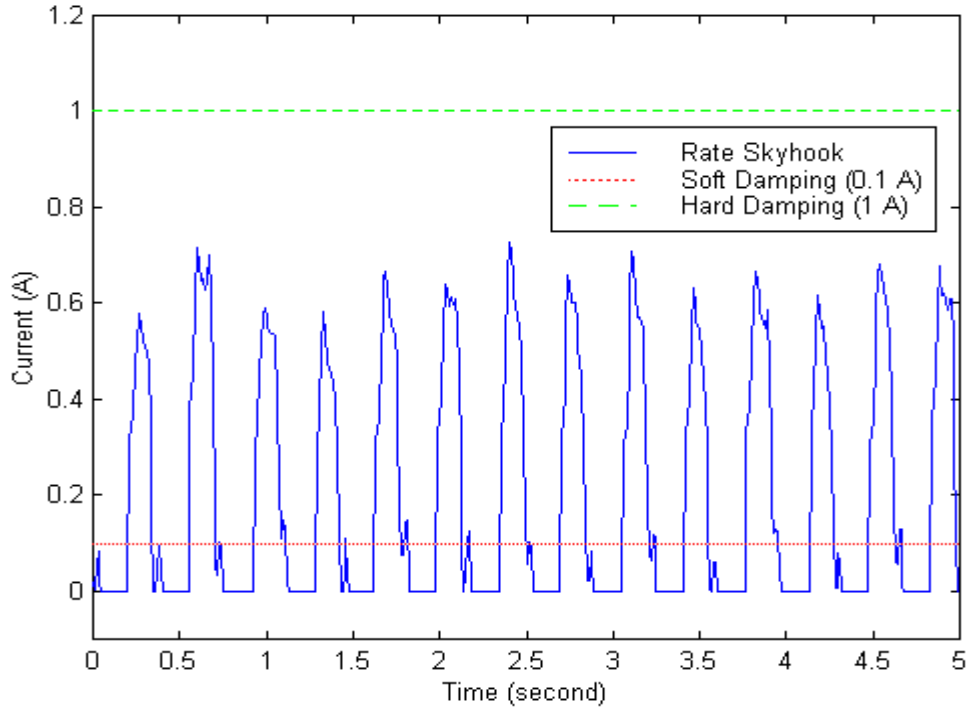

Figure 4.16 Current Supplied to the MR Damper
for Pure Tone Excitation in Time Domain

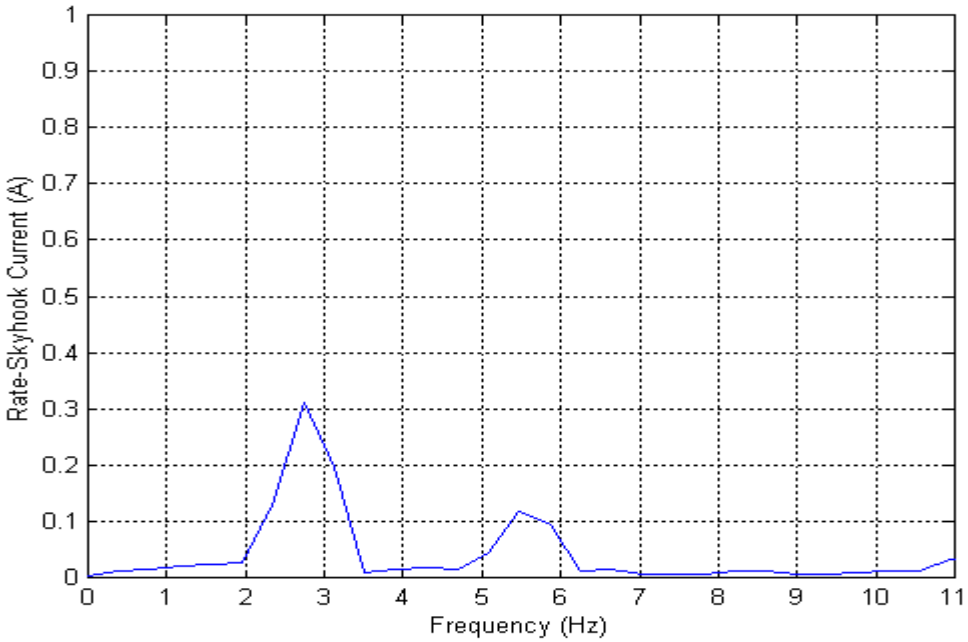

Figure 4.17 Power Spectrum of the Electrical Current to the MR Damper for Skyhook Control

The time history of the electrical current to the damper shown in Fig. 4.16 shows that the currents from the skyhook control policy are tuned alternatively between zero Amperes and non-zero Amperes according to the velocities, while the constant damping cases have constant currents. All of the cases have only one thing different that is the control signal of the current to the MR damper. Thus, it can be inferred that the nonlinear dynamic responses are strongly related to this signal, but not from the nonlinearities of the MR damper. In the following, we will try to use the signal flow diagram, shown in Fig. 4.18, to explain how the skyhook produces the higher harmonics.

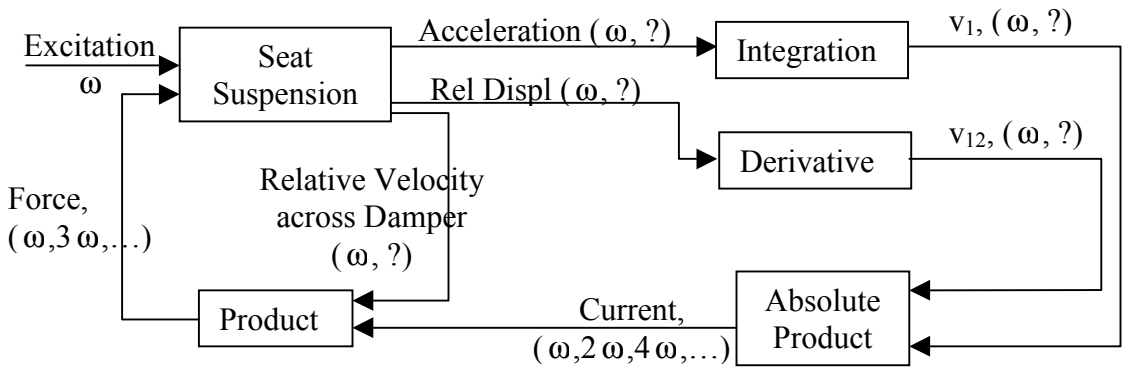

Figure 4.18 Signal Flow for Semiactive Skyhook Control

According to Fig. 4.18, if a pure-tone excitation signal with a frequency of 1.4 Hz is used to vibrate the seat and the seat suspension is nearly 1.4 Hz, then it is expected that dynamic responses of the system will have a relatively large peak at 1.4 Hz. This phenomenon is clearly apparent in Fig. 4.15.

As shown in Fig. 4.16, the current is set to be zero Amperes when the sign of the product of the absolute velocity and relative velocity is negative, otherwise, it is the absolute value of the absolute velocity. This implies that the current changes at twice the predominant frequency of the absolute velocity. For instance, for our system this is 2 x 1.4 = 2.8 Hz. As is clearly shown in Fig 4.17. Therefore, as shown in Fig. 4.18, the damping force can be characterized by

$$F = (V_{rel} \sin \omega t) \sum_{i=2,4...}^{\infty} I_i \sin(i\omega\, t) = \sum_{k=1,3...}^{\infty} F_k \cos(k\omega t) \qquad (4.10)$$

Equation (4.10) implies that the damping force has periodic components that are odd multiples of the excitation frequcncy. This was the phenomenon that we clearly observed in Fig. 4.15. The first periodic component that occurs at the same frequency as the system resonance is necessary for controlling the resonance response of the system. The other periodic components appear as higher harmonics and sometimes can excite unwanted dynamics of the system. It is, however, important to note that as shown in Eq. (4.10) the first harmonic and the higher harmonics are strongly tied together, and one cannot occur without the other. In other words, if larger forces are needed at the resonant frequency of the system, then larger higher harmonic peaks will result. If the higher harmonics are not acceptable for a system, then the damping force at the resonant frequency must be sacrificed to achieve lower higher harmonic peaks.

4.3.2 Analysis of Experimental Data in Time Domain

In this section, we will analyze the seat suspension experimental data in the time domain, in order to further highlight the seat response due to skyhook control.

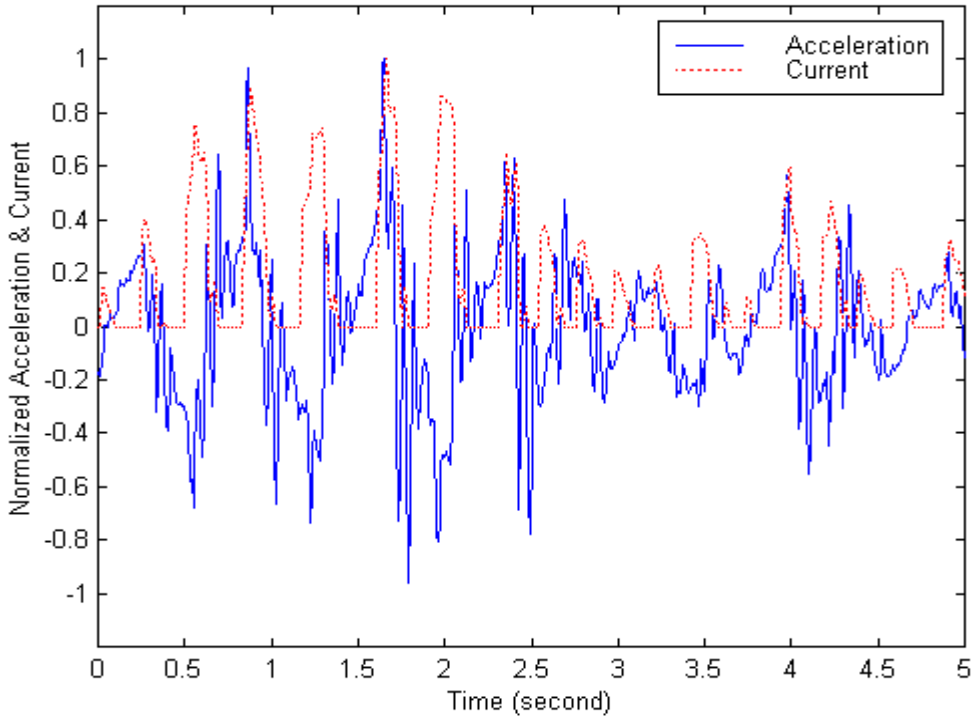

Figure 4.19 Acceleration and Damper Current Time Reponse
for ISO2 Excitation in Time Domain

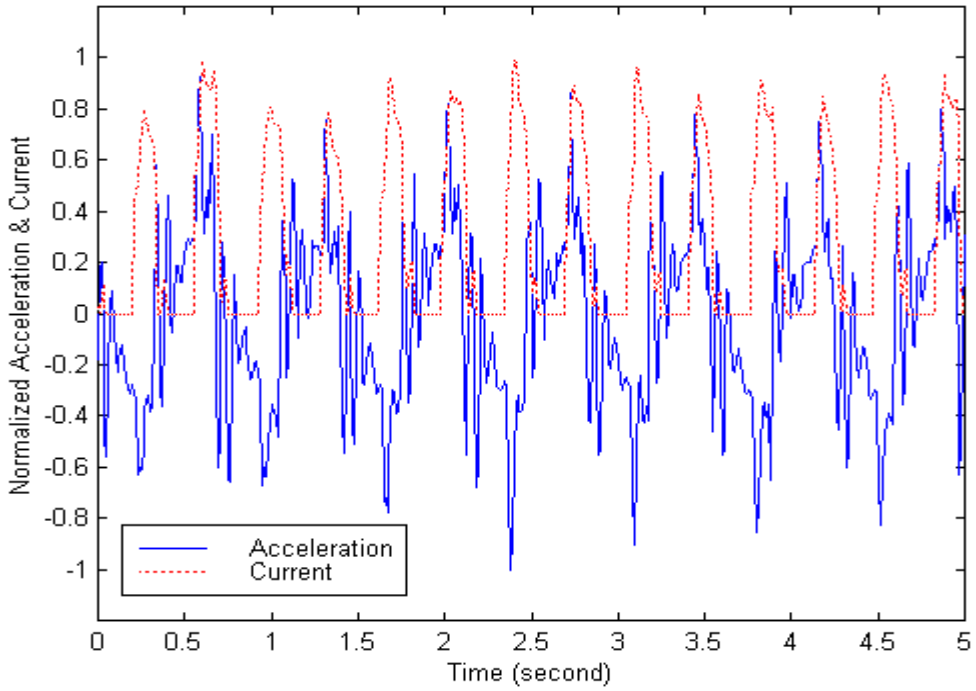

Figure 4.20 Acceleration and Damper Current Time Response
for Pure Tone Excitation in Time Domain

The results in Figs. 4.19 and 4.20 show a number of large peaks that occur concurrently with the switching of the dampers from off- to on-state. Such acceleration jumps introduce high jerks in the seat dynamic response and cause an uncomfortable sensation for the person riding on the seat. As such, determining the source of the dynamic jerks and eliminating them can signifigantly improve the subjective dynamic responses of the seat.

4.3.2.1 Dynamic Jerk Analysis

A three-dimensional surface plot of skyhook control is shown in Fig. 4.21 for damper force, relative velocity, and absolute velocity. It shows that in the second and fourth quadrant, when the relative and absolute velocity have opposite sign, the damper force is zero. Otherwise it is proportional to absolute velocity. Figure 4.21 is a graphical representation of Eq. (4.1). As highlighted in Fig. 4.21, the damping force jumps sharply at the transitions between quadrants corresponding to the relative velocity zero-crossings. The force discontinuity causes the acceleration jumps or jerks.

The phenomena observed in Fig. 4.21 can be further analyzed by studying Fig. 4.22. This figure shows that jerks correspond to sharp transitions of the damper current at the zero-crossings of the estimated relative velocity that has a phase-lag with respect to the true relative velocity, but the phase error due to the estimated absolute velocity does not cause sharp transitions of the damping force, as shown in Fig. 4.22. The errors in the relative velocity can be due to the rate filter explained earlier, or other estimations that may be used in the system. The approaches for reducing or eliminating jerks can be:

1. Improve the rate filter accuracy by increasing the break frequency to obtain a more accurate estimate of the relative velocity. This method is not very practical, due to the necessity of higher-speed hardware and possibility of introducing higher-frequency noise.
2. Employ some analytic continuous functions instead of the binary logic skyhook control, shown in Eq. (4.1), to avoid the damping force discontinuity.

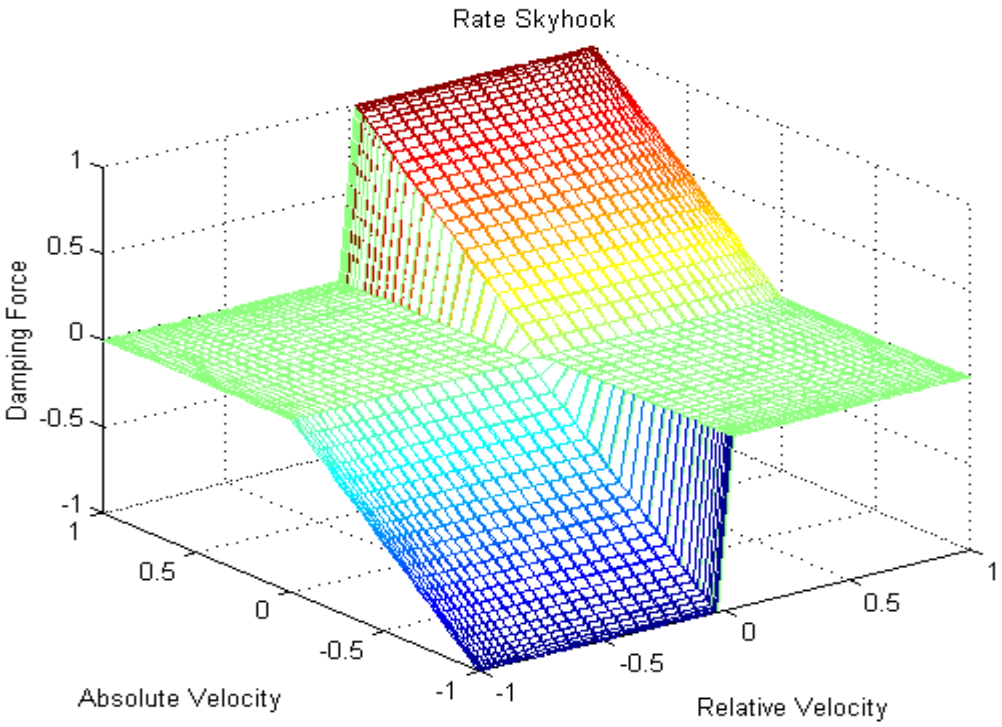

Figure 4.21 Surface Plot of Skyhook Control Damper Force

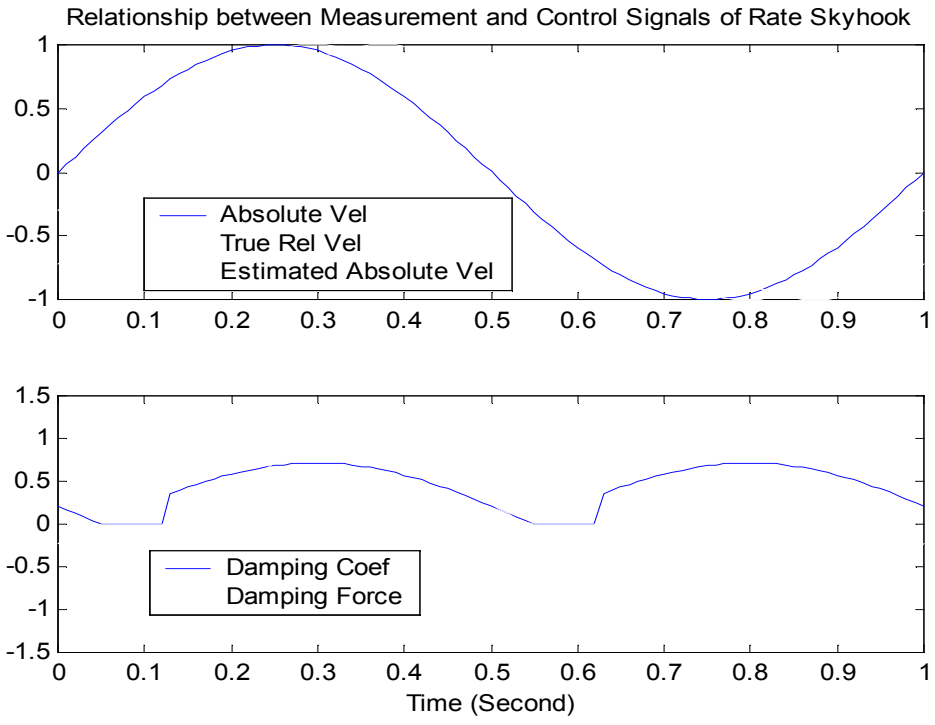

(a)

Figure 4.22 Effect of Estimate Errors of (a) Absolute Velocity;
(b) Relative Velocity on Damping Force

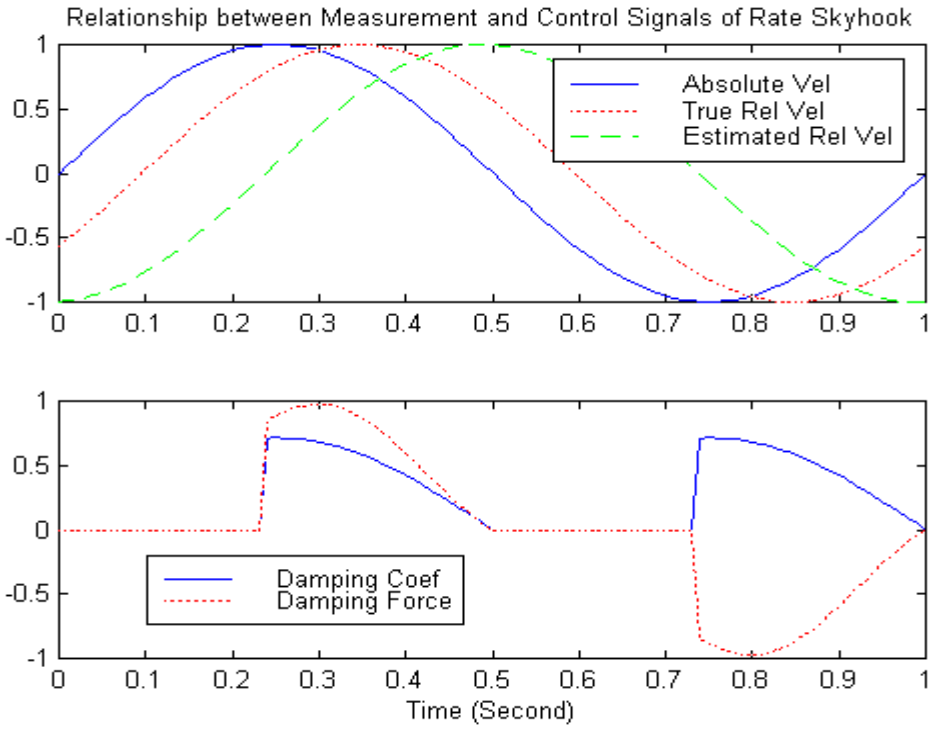

(b)

Figure 4.22 Effect of Estimate Errors of: (a) Absolute Velocity;
(b) Relative Velocity; on Damping Force

3. Modify the skyhook control policy to enable smooth transition of damper current, even when the damper is not at its true relative velocity zero crossing.

In the next sections, we will demonstrate how the two items 2 and 3 from above can reduce dynamic jerks due to the skyhook control.

4.4 Continuous Skyhook Function

A continuous equation is proposed to mimic the skyhook Eq. (4.1) as follows

$$I = I_s + \frac{e^{f} - e^{-f}}{I_{on}e^{f} + I_{off}e^{-f}} \tag{4.11}$$

where I_s, I_{off} and I_{on} are constant.

The constants I_s and I_{on} are small as compared to I_{off}, i.e., $I_s << I_{off}$ and $I_{on} << I_{off}$. The exponential power f represents the switching function of skyhook, and is a funciton of relative velocity, absolute velocity or any other appropriate measure. For example, it can be

$$f = Kv_1 v_{12}$$

where K is a positive constant.

Figure 4.23 shows a surface plot of the damping force with respect to the absolute and relative velocity. In Fig. 4.23 it can be observed that smooth transition of the damping force from one quadrant to another can be achieved, as compared to Fig. 4.21. A similar difference can be observed between Figs. 4.24 and 4.22. Both Figs. 4.23 and 4.24 indicate that the skyhook function control can yield substantially lower dynamic jerks.

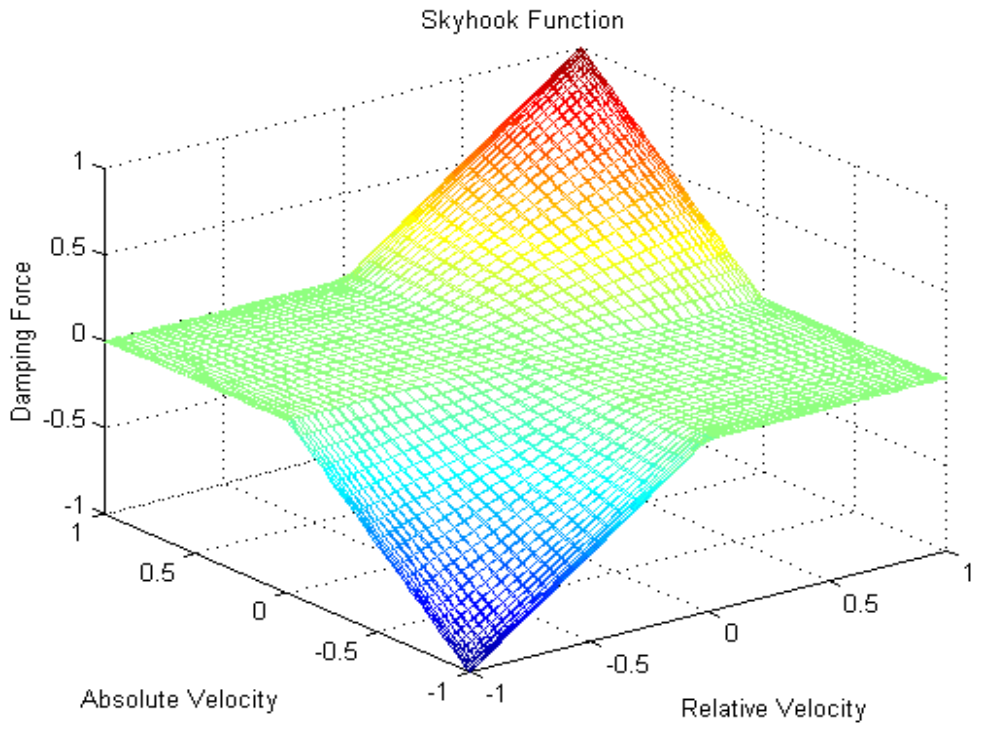

Figure 4.23 Surface Plot of Skyhook Function Control Damper Force

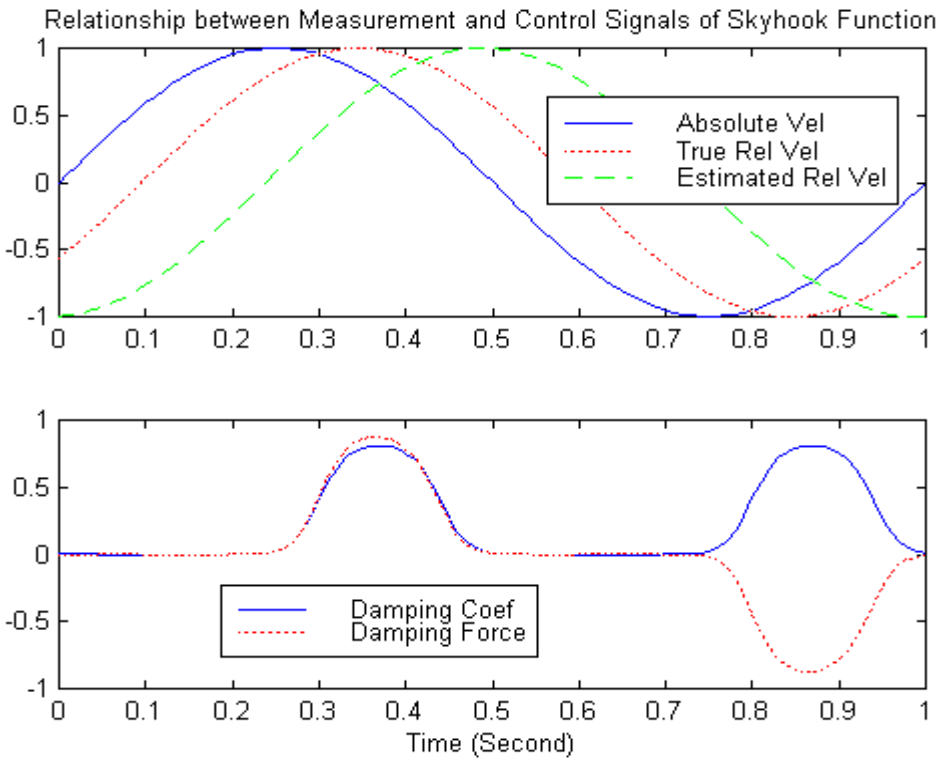

Figure 4.24 Effect of Relative Velocity Errors on Damping Force Discontinuity

4.5 No-Jerk Skyhook

Alternative formulation to Eq. (4.1) for reducing dynamic jerk is

$$I = \begin{cases} K|v_1 v_{12}| & v_1 v_{12} \geq 0 \\ 0 & v_1 v_{12} < 0 \end{cases} \tag{4.12}$$

where K is a constant gain. This formulation is quite similar to the skyhook control shown in Eq. (4.1), except that the damper current is a function of both absolute and relative velocity. As will be shown in Fig. 4.25 and 4.26, including relative velocity eliminates damping force discontinuity and dynamic jerks.

Figure 4.25 shows that the damping force has smooth transition between four quadrants, but in Fig. 4.21 the force has jumps at the zero-crossings of the relative velocity. Further, we can observe a similar difference between Figs. 4.22 and 4.26. Therefore, continuous force can avoid jerks.

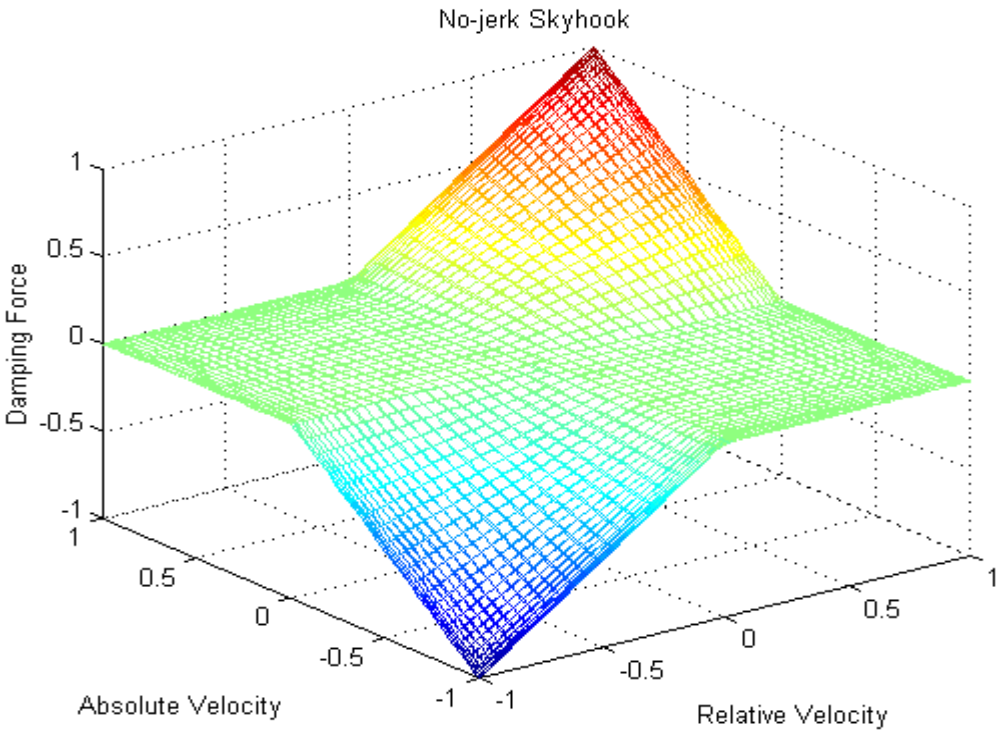

Figure 4.25 Surface Plot of No-Jerk Skyhook Control Damper Force

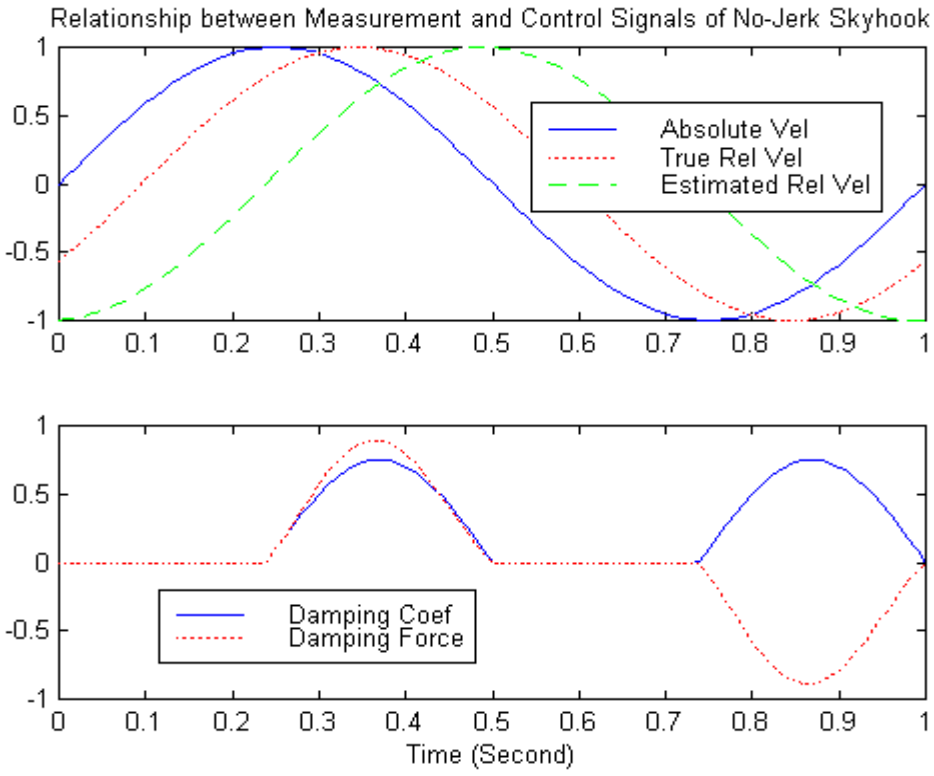

Figure 4.26 Effect of Relative Velocity Errors on Damping Force Discontinuity

4.6 Dynamic Evaluation of Modified Skyhook Controls

Similar to the implementation of the modified skyhook, both new modified skyhooks are programmed in Simulink, and then downloaded into the dSPACE AutoBox for testing. The testing results are shown from Figs. 4.27 to 4.30.

Firstly we investigate the currents to the MR damper as shown in Figs. 4.28 and 4.30. It is no surprise that the skyhook function is very similar to the no-jerk skyhook. Both improved control policies have smooth transition of the current from off- to on-state for the MR damper, because the new modified skyhook control policies take advantage of the fact that at least one velocity changes smoothly from on- to off-state or vice versa. Thus, the new modified skyhooks can produce smooth dynamic responses. Figures 4.27 and 4.29 show that both no-jerk skyhook and skyhook function control policies can produce cleaner dynamic responses without those obvious jerks due to the phase lag of the relative velocity estimate, because these new control policies do not produce any damping force discontinuity. Further, such modifications, especially no-jerk skyhook, do not need any extra hardware but absolutely improve the product performance.

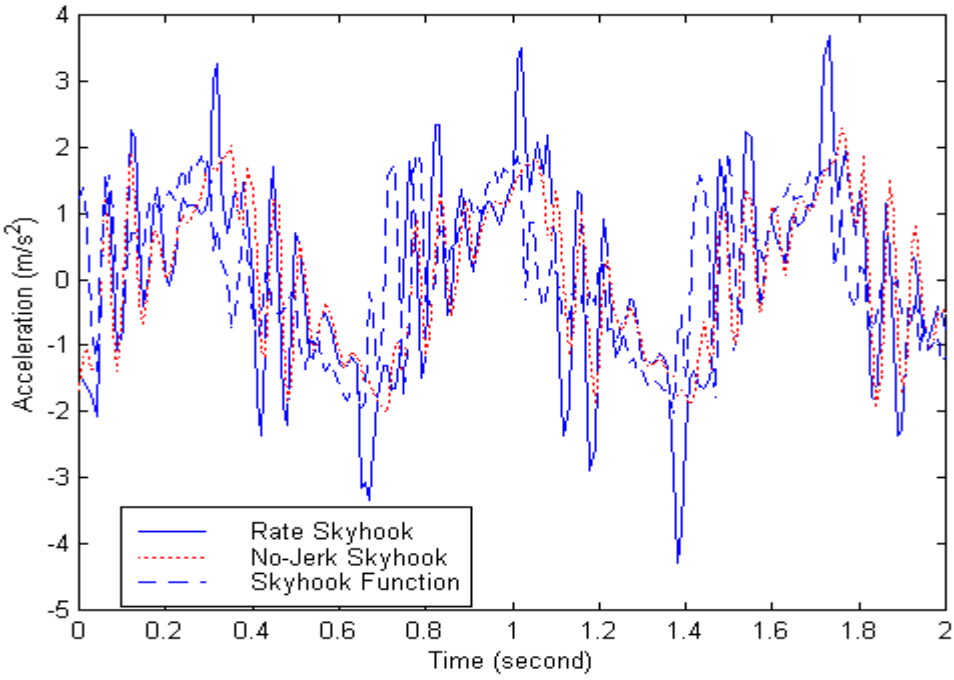

Figure 4.27 Comparison of Accelerations with Different Controls under 1.45-Hz Pure Tone Excitation

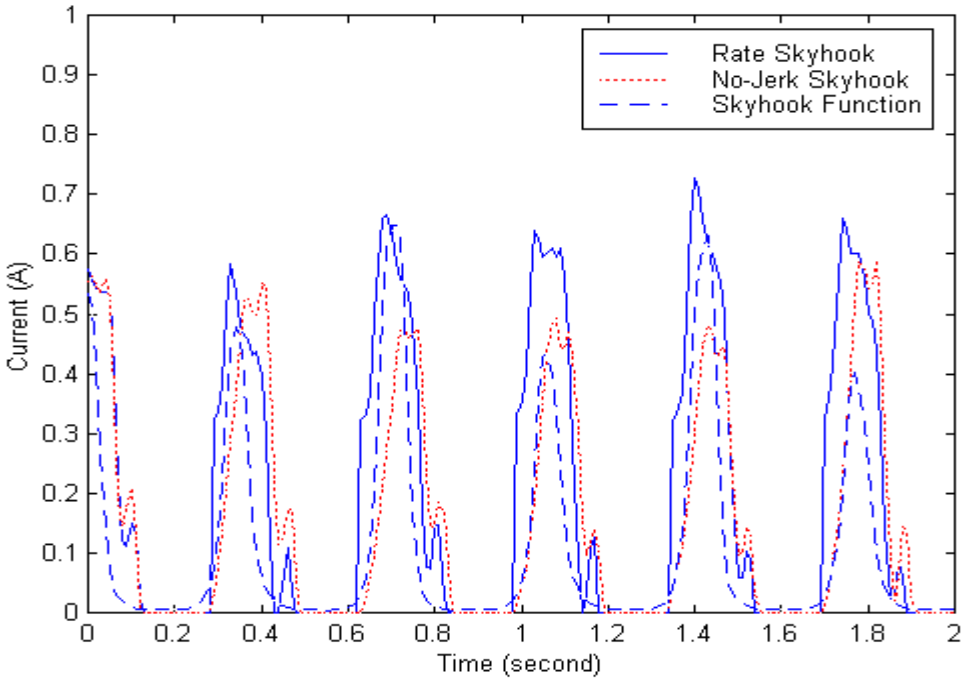

Figure 4.28 Comparison of Currents with Different Controls
under 1.45-Hz Pure Tone Excitation

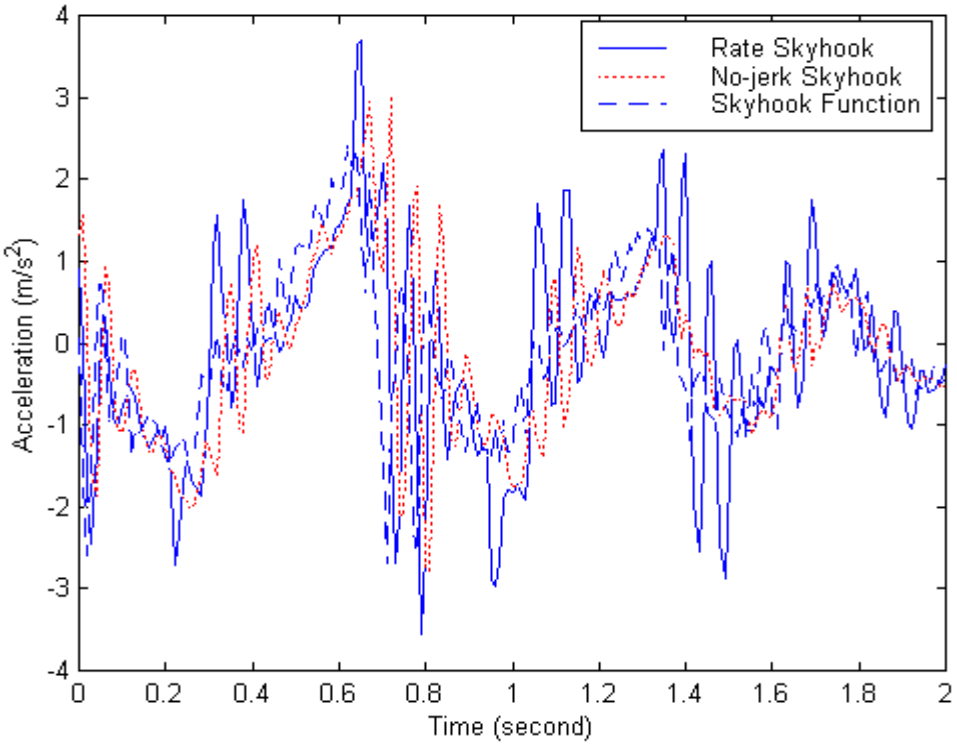

Figure 4.29 Comparison of Accelerations with Different Controls under ISO2 Excitation

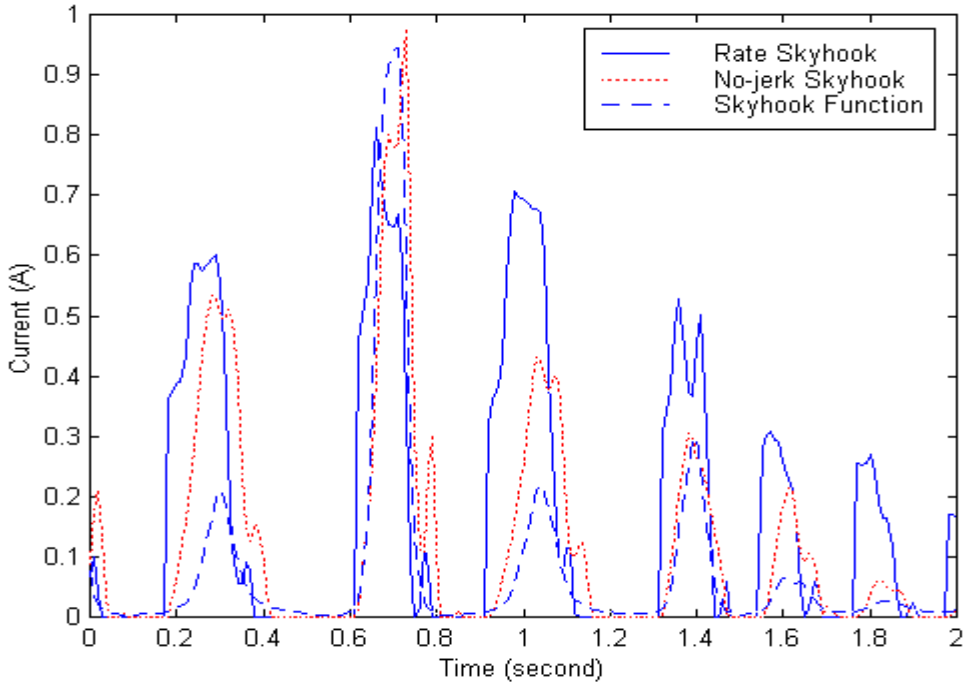

Figure 4.30 Comparison of Currents with Different Controls under ISO2 Excitation

From the testing results, we conclude that the new modified skyhooks can avoid the jerky responses, but the higher harmonics are still existing in the dynamic responses. Therefore, it is necessary to explore new damping tuning methods.

4.7 Summary

The practical implementation of semiactive skyhook control in a seat suspension system was presented. Upon presenting the approach that is used for implementing the skyhook control, the dynamic response of the seat was evaluated.

It was shown that the rate skyhook control caused a secondary peak three times the resonant frequency of the system. Further it was shown that skyhook control introduced a series of large acceleration peaks (i.e., jerk) to the measurements on the seat. The sources of each of their dynamic phenomena were investigated and two new modified skyhook control policies, referred to as no-jerk skyhook and skyhook function, were suggested for reducing the jerk caused by skyhook control.